J. Fluid Mech. (2009), *vol.* 619, *pp.* 367–376.
doi:10.1017/S0022112008004862 Printed in the United Kingdom

The shape of submarine levees: exponential or power law?

V. K. BIRMAN[1], E. MEIBURG[1]† AND B. KNELLER[2]

[1]Department of Mechanical Engineering, University of California, Santa Barbara, CA 93106, USA

[2]Department of Geology & Petroleum Geology, University of Aberdeen, Aberdeen AB24 3FX, UK

(Received 18 March 2008)

Field observations indicate that the height of submarine levees decays with distance from the channel either exponentially or according to a power law. This investigation clarifies the flow conditions that lead to these respective shapes, via a shallow water model for the overflow currents that govern the levee formation. The model is based on a steady state balance of sediment supply by the turbidity current, and sediment deposition onto the levee, with the settling velocity and the entrainment rate appearing as parameters. It demonstrates that entrainment of ambient fluid is the determining factor for the levee shape. For negligible entrainment rates, levee shapes tend to exhibit exponential profiles, while constant rates of entrainment or detrainment result in power law shapes. Interestingly, whether a levee has an exponential or a power law shape is determined by kinematic considerations only, viz. the balance laws for sediment mass and fluid volume. We find that the respective coefficients governing the exponential or power law decay depend on the settling speeds of the sediment grains, which in turn is a function of the grain size. Two-dimensional, unsteady Navier–Stokes simulations confirm the emergence of a quasi-steady state. The depositional behaviour of this quasi-steady state is consistent with the predictions of the shallow water model, thus validating the assumptions underlying the model, and demonstrating its predictive abilities.

1. Introduction

The floor of the deep sea exhibits submarine channels (e.g. Normark, Posamentier & Mutti 1993). These channels form the conduits by which sediment is transported into deep marine basins by turbidity currents (gravity-driven turbid mixtures of sediment and water) that may be catastrophic, lasting only for a few hours or sustained over periods of days or weeks (Normark & Piper 1991; Piper & Savoye 1993; Pirmez & Imran 2003). The channels range from a few metres to a few kilometres in width, up to several hundreds of metres deep and may be tens to thousands of kilometres in length (Clark & Pickering 1996; Huebscher *et al.* 1997; Babonneau *et al.* 2002). Many of these channels are flanked by levees, analogous to natural river levees, formed by deposition of sediment from parts of the flows that spilled out of the channels (e.g. Hiscott, Hall & Pirmez 1997). Since individual levees may achieve thicknesses of tens to a few hundreds of metres, and widths perpendicular to the channel commonly of several kilometres to tens of kilometres, they contain very large cumulative masses of

† Email address for correspondence: meiburg@engineering.ucsb.edu

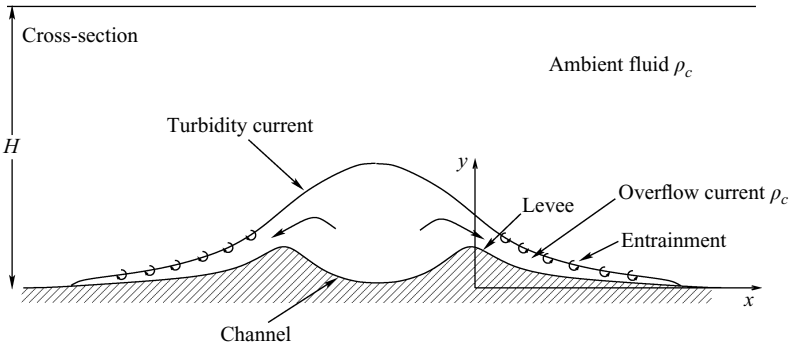

FIGURE 1. Cross-section of a turbidity current propagating along a submarine channel flanked by levees. The shape of these levees is governed by the depositional behaviour of lateral overflow currents, which may entrain ambient fluid. The vertical scale is greatly exaggerated.

sediment. Moreover, stacked channel–levee systems (in which younger channels and their levees occupy the topographically lower regions between older levees) form a high proportion of the thick, dominantly fine-grained sediment accumulations of the continental slope and rise, especially offshore from major river systems such as the Indus, Bengal, Congo and Amazon (Kolla & Schwab 1995; Huebscher *et al.* 1997; Babonneau *et al.* 2002).

The typical shape of a submarine channel levee is illustrated schematically in the cross-section shown in figure 1. On the basis of observations of levees on the modern sea floor, Skene, Piper & Hill (2002) considered that the thickness of the sediment accumulation forming the levee decays exponentially away from the channel. However, Kane *et al.* (2007) subsequently established a power law decay in thickness of ancient submarine levee deposits, and recent work using seismic surveys in the shallow subsurface below the sea floor suggests that both types of thickness decay may occur (Kneller *et al.*, in preparation). The present investigation aims to clarify the differences in flow conditions over the levee that may result in these respective levee shapes.

While there have been only limited attempts to model sediment deposit profiles in the direction perpendicular to the main flow, a number of investigations have addressed the issue of streamwise variations in the deposit thickness, e.g. the shallow water analysis by Bonnecaze, Huppert & Lister (1993). Hallworth *et al.* (1993) draw attention to the role of entrainment in such flows, and develop corresponding scaling laws via dimensional analysis. A recent review of scaling analysis approaches to deposition problems is provided by Srivatsan, Lake & Bonnecaze (2004).

The case of turbidity currents propagating down slopes was addressed by Bonnecaze & Lister (1999). Dade, Lister & Huppert (1994) develop a simplified model for sedimenting surges propagating down a slope, by extending earlier work of Beghin, Hopfinger & Britter (1981) for corresponding non-depositing currents. By incorporating a fluid entrainment rate in the form of a fraction of the average surge speed, their model predicts a region of power law decay, followed by an exponential decay region further downstream. For a more general discussion of the role of entrainment in geophysical fluid flows, cf. Turner (1968, 1986). An overview over these investigations, and the underlying tools such as box models and shallow water equations is provided by Huppert (1998). This paper also addresses the case of polydisperse suspensions, and the role of a less dense interstitial fluid.

More recent efforts to model turbidity currents and the deposits they form have been based on three-dimensional Navier–Stokes simulations, cf. Necker *et al.* (2002, 2005). These authors observe good agreement with corresponding laboratory data of de Rooij & Dalziel (1998) regarding both temporal and spatial development of the deposit layer thickness in the streamwise direction. In the following, we will employ both shallow water equations and Navier–Stokes simulations towards analysing thickness variations of submarine levees perpendicular to the propagation direction of the turbidity current.

Section 2 develops a shallow water model for the overflow current. This model is based on a steady state balance between the sediment supplied to the overflow current by the main turbidity current, and the deposition of sediment onto the levee by the overflow current. The rate at which the overflow current entrains ambient fluid is seen to play a crucial role in determining the levees decay rate. Two-dimensional, unsteady numerical Navier–Stokes simulations are conducted in § 3, and their results are discussed in § 4. A comparison between the simulation results and the shallow water model is provided in § 5.

2. Model

In order to analyse the formation of levees, we focus on a model of the cross-section of a deeply submerged turbidity current, cf. figure 1. While the main flow direction of the turbidity current is out of the plane, a portion of the current overflows its banks in the lateral direction. Gradients in the main flow direction of the current are assumed to be small, so that they are negligible in comparison with gradients in the cross-sectional plane. We assume that the turbidity current is maintained over sufficiently long times for an approximately steady state balance to form between the supply of sediment from the main turbidity current to the overflow current, and its loss through sedimentation. Erosional effects are not considered in the present analysis. Note that, for this reason, the model to be developed in the following would not be applicable to the downstream development of the channel bed, whose development is governed by a balance of erosion and deposition. The quasi-steady, spatial distribution of the sediment deposit rate in the spanwise x-direction will then determine the shape of the levee. Field observations from ancient levees now exposed onland, and from the ocean confirm the generally quasi-steady (though episodic) and generally non-erosive nature of flow over deep marine levees (Hiscott *et al.* 1997; Kane *et al.* 2007).

In deriving a set of shallow water equations governing the overflow current, we make several simplifying assumptions. The vertical velocity is assumed to be sufficiently small so that it can be neglected compared to the spanwise velocity u. We furthermore assume that the overflow current is well mixed over its entire vertical height h, so that both the sediment concentration, ϕ, and the spanwise velocity u are functions of the spanwise coordinate x only. Hence the current is fully characterized by $u(x)$, $h(x)$ and $\phi(x)$.

Let us consider a control volume $ABCD$ of the flow, cf. figure 2. Since a typical terrain slope is of the order of 2 degrees at most, and usually a lot smaller than that, we neglect its effect and assume that the current flows over a horizontal bottom BC, cf. also Britter & Linden (1980), Bonnecaze & Lister (1999) and Birman *et al.* (2006). Nonetheless, it may be possible that for some levees this small slope might suffice to generate transitional flow. The inflow of sediment through boundary AB is then balanced by sediment deposition along BC, and by the outflow of sediment through

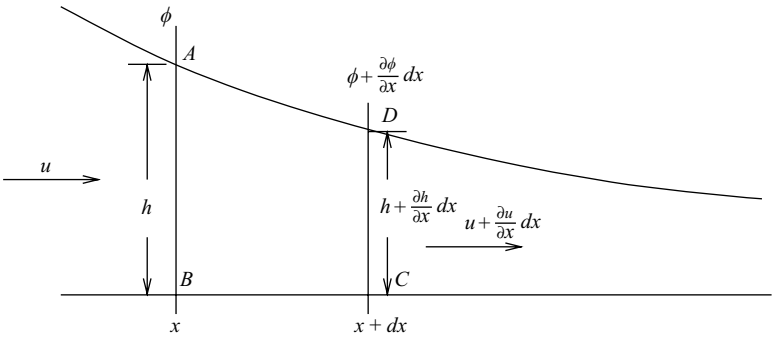

FIGURE 2. The shallow water model is obtained from the conservation principle for sediment, fluid and momentum in the control volume $ABCD$.

CD. We obtain

$$\frac{\partial(\phi u h)}{\partial x} = -\phi u_s, \tag{2.1}$$

cf. Bonnecaze *et al.* (1993). Here, u_s is the constant settling velocity of the monodisperse sediment grains.

Balancing fluid inflow through AB with fluid outflow through CD and entrainment or detrainment of fluid (not sediment) through AD yields

$$\frac{\partial(u h)}{\partial x} = E(x), \tag{2.2}$$

where $E(x)$ is the entrainment flux across the interface of the current and the ambient fluid. Here the volume fraction of the sediment is neglected, consistent with estimates of suspended sediment concentration of a few volume per cent (e.g. Bowen, Normark & Piper 1984).

A corresponding balance can be established for the conservation of momentum. By neglecting the effects of viscosity, bottom friction and momentum entrainment, we obtain

$$\frac{\partial(u^2 h)}{\partial x} + \frac{g'}{2\phi_0}\frac{\partial(\phi h^2)}{\partial x} = 0. \tag{2.3}$$

Here the first term indicates the derivative of the momentum flux, while the second term represents the hydrostatic pressure gradient. The reduced gravity g' is defined as $g' = \pi(\rho_p - \rho_a)\phi_0 d_p^3 g/6\rho_a$, with ρ_p denoting the density of the sediment material, ρ_a the ambient fluid density, d_p the sediment grain diametre and ϕ_0 the number concentration of the sediment grains in the turbidity current.

As shown in figure 1, the origin of the coordinate system is located at the crest of the levee. We complete the flow model by specifying boundary conditions at $x = 0$ of the form $h(0) = h_0$, $\phi(0) = \phi_0$ and $u(0) = u_0$.

Equations (2.1), (2.2) and (2.3) specify the solutions for $u(x)$, $h(x)$ and $\phi(x)$, with the Stokes settling velocity u_s and the entrainment (or detrainment) rate $E(x)$ as parameters. The entrainment rate can depend on a number of flow features, such as the overall Reynolds number of the flow, the particle settling velocity or the local sediment concentration. In order to clarify the influence of $E(x)$ on the character of the overflow current, and consequently on the levee shape, we will focus on the two representative cases in which we assume either $E(x) = 0$ (zero entrainment) or $E(x) = E_0$ (constant entrainment or detrainment). For each of these cases, we will

determine the profile of the sediment concentration as a function of the spanwise x-distance. This, in turn, will yield the quasi-steady sedimentation rate, and hence the levee height, as functions of x.

2.1. *Zero entrainment*

By employing the chain rule, we can rewrite the sediment conservation equation (2.1) as

$$\phi \frac{\partial (uh)}{\partial x} + uh \frac{\partial \phi}{\partial x} = -\phi u_s. \tag{2.4}$$

For $E(x) = 0$, the fluid conservation equation (2.2) yields $uh = (uh)_0 = A_0$, so that equation (2.4) yields for the quasi-steady, depth-averaged sediment concentration

$$\phi(x) = \phi_0 \mathrm{e}^{-(u_s/A_0)x}. \tag{2.5}$$

Hence, without entrainment the sediment concentration in the overflow current decays exponentially with the distance from the levee crest. Since the settling velocity is independent of the sediment concentration, the rate at which the overflow deposits sediment decays exponentially as well. Finally, since the flow field is steady, the height of the levee formed by this deposit also decays exponentially, with an exponent proportional to the settling velocity of the sediment grains. Note that in the above conservation equations u and h do not appear individually, but only as the product uh. Consequently, the levee shape can be determined from the fluid and sediment conservation equations alone, i.e. from kinematic considerations, while the momentum balance does not enter. However, the momentum balance needs to be invoked if u and h are to be determined individually.

2.2. *Constant entrainment*

For $E(x) = E_0$, the fluid conservation equation (2.2) yields $uh = E_0 x + B_0$, so that the expanded sediment conservation equation (2.4) simplifies to

$$E_0 \phi + (E_0 x + B_0) \frac{\partial \phi}{\partial x} = -\phi u_s. \tag{2.6}$$

By rescaling the spanwise coordinate x and shifting its origin such that $\hat{x} = E_0 x + B_0$, the solution in terms of the rescaled distance $\hat{x}$ takes the form

$$\phi(\hat{x}) = \phi_0 (B_0/\hat{x})^{\frac{u_s + E_0}{E_0}}. \tag{2.7}$$

Hence, following the same line of reasoning as for the zero entrainment case, an overflow current with constant entrainment of ambient fluid forms a levee whose height exhibits a power law decay. Note that E_0 can be positive (net entrainment) or negative (net detrainment). The fastest possible detrainment of fluid from the overflow current occurs when the interface separating the overflow current from the ambient fluid shifts downward with the settling velocity of the sediment grains, so that $E_0 = -u_s$. In this case, $\phi(x)$ is constant. For $E_0 > -u_s$, ϕ is a decreasing function of x, so that the sediment becomes more diluted as it moves away from the centre of the turbidity current.

3. Navier–Stokes simulations

To test the predictions obtained from the above shallow water model, we conduct time-dependent, two-dimensional Navier–Stokes simulations in the Boussinesq limit. The setup shown in figure 3 captures the flow in a cross-section perpendicular to the

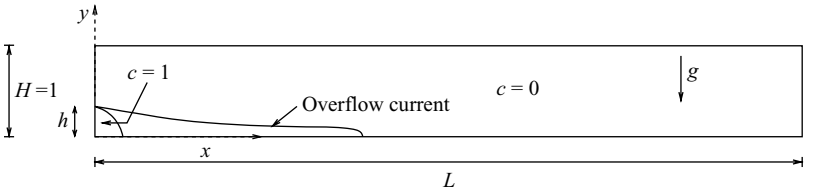

FIGURE 3. A domain of length L and height H is used to simulate the overflow current. The elliptical region in the bottom left corner represents the cross-section of main turbidity current. In this region, the dimensionless sediment concentration is maintained at $c=1$ for all times. This sediment feeds a depositional overflow current propagating to the right, which eventually reaches a steady state whose characteristics determine the levee shape.

main propagation direction of the turbidity current: a computational domain of width L and height H is, for the most part, initially filled with clear fluid of density ρ_a. The small elliptical region in the bottom left-hand corner of the domain represents the cross-section of the turbidity current. In this region we maintain a sediment number concentration $c=c_0$ for all times. Note that the shape of this region has a negligible influence on the quasi-steady flow that evolves for long times.

For dilute mixtures, the governing Navier–Stokes equations are derived and discussed in Necker *et al.* (2002, 2005) and Blanchette *et al.* (2005). Those authors show that the conservation of mass, momentum and sediment is described by

$$\frac{\partial u_l}{\partial x_l} = 0, \tag{3.1}$$

$$\frac{\partial u_i}{\partial t} + u_l \frac{\partial u_i}{\partial x_l} = -\frac{\partial p}{\partial x_i} + \frac{1}{Re}\frac{\partial^2 u_i}{\partial x_l \partial x_l} + c e_i^g, \tag{3.2}$$

$$\frac{\partial c}{\partial t} + \left(u_l + u_s e_l^g\right)\frac{\partial c}{\partial x_l} = \frac{1}{ReSc}\frac{\partial^2 c}{\partial x_l \partial x_l}, \tag{3.3}$$

where the summation convention has been used. Here, lengths and velocities are non-dimensionalized with the domain height H and the buoyancy velocity $u_b=\sqrt{g'H}$, respectively. The latter provides a characteristic scale for the velocity induced by the density variations. Note that any length scale could have been chosen to define the buoyancy velocity, since the only goal is to determine whether the levee decays exponentially or algebraically. Time and pressure scales are provided by H/u_b and $\rho_a u_b^2$, while concentration is normalized by c_0. The unit vector in the direction of the gravitational acceleration is denoted by e_i^g. As dimensionless parameters we obtain the Reynolds number $Re=u_b H/\nu$ and the Schmidt number $Sc=\nu/\kappa$, in addition to the normalized settling velocity u_s. Here, ν and κ denote an effective eddy viscosity and diffusivity, respectively, for momentum and the sediment grains. Since for a complex flow such as the present one (particle-laden fluid with varying sediment concentration, near a sediment bed), we do not know the precise spatial dependence of ν and κ, we assume that, as a first approximation, they are spatially invariant. This approach avoids the introduction of additional dimensionless parameters.

The left domain boundary is treated as symmetry planes. The same treatment is applied to the right boundary, which is justified since the current decays long before reaching this boundary. A no-flux condition for the sediment concentration is enforced at the top boundary, while the sediment grains are allowed to settle out of the computational domain at the bottom boundary via an 'outflow' boundary condition (Necker *et al.* 2002, 2005). The change in the shape of the bottom boundary

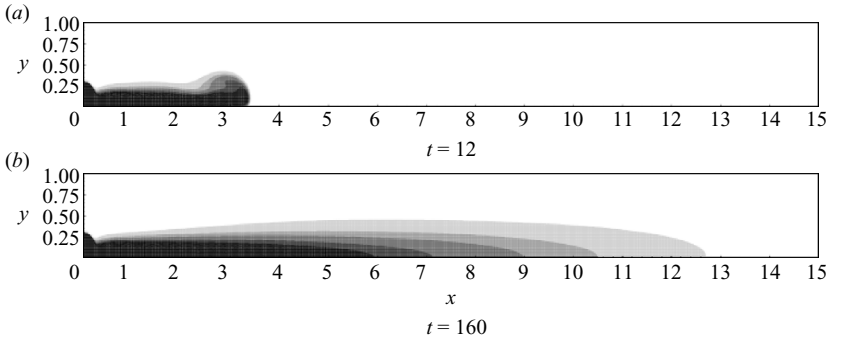

FIGURE 4. sediment concentration contours of an overflow current with $Re = 2000$, $Sc = 1$ and $u_s = 0.01$ at $t = 12$ and 160. The contour levels displayed are $\phi = 0.01$, 0.05, 0.1, 0.2, 0.3, 0.4, 0.5, 0.6, 0.7 and 0.8. The steady state is reached around $t = 160$.

due to accumulating sediment is neglected. For the fluid velocity, we employ no-slip (slip) conditions at the top and bottom (left and right) boundaries. Initially, the fluid is at rest everywhere. We solve the above equations in the vorticity-streamfunction formulation, employing a pseudo-spectral approach in the x-direction, 6th order compact finite differences in the y-direction, and a 3rd order, low storage Runge-Kutta scheme. Further details of the computational technique can be found in Härtel, Meiburg & Necker (2000).

We perform time-dependent numerical simulations for the above setup, until a steady state overflow current has evolved. The functions $h(x)$, $\phi(x)$ and $u(x)$ obtained from this steady state can then be compared directly with the shallow water model results.

4. Simulation results

Numerical simulations have been performed for the three different settling velocities $u_s = 0.005$, 0.01 and 0.03, along with $Re = 2000$ and 10 000, and $Sc = 1$. As dimensionless values, these settling velocities indicate fractions of the characteristic velocity. Since the velocity of the overflow current at the levee crest is of the same order as the buoyancy velocity, the dimensionless settling velocity values roughly correspond to fractions of the overflow current velocity. Hence, depending on the dimensional velocity of the overflow current, they may correspond to typical values for silt or sand. The value of $Re = 2000$ was chosen to be sufficiently large for the steady state of the flow to be effectively independent of Re, so that the results can be compared with the shallow water analysis.

To study the effects of larger entrainment, we performed one simulation with $u_s = 0.01$, $Re = 2000$ and $Sc = 0.1$. Figure 4 displays representative sediment concentration contours for the flow with $u_s = 0.01$ and $Sc = 1$. The overflow current initially forms close to the left boundary and subsequently propagates along the bottom wall. As the sediment settles out, the current gradually loses its driving force until it finally reaches its steady, maximum runout length. In this state, the supply of sediment from the turbidity current is balanced by the loss of sediment due to deposition along the bottom surface, which determines the shape of the levee.

We consider the tip location x_{tip} of the overflow current as the foremost point of the $c = 0.01$ contour. Figure 5(a) shows x_{tip} as function of time for different settling speeds. The asymptotic formation of a steady state is clearly seen. Per definition, we

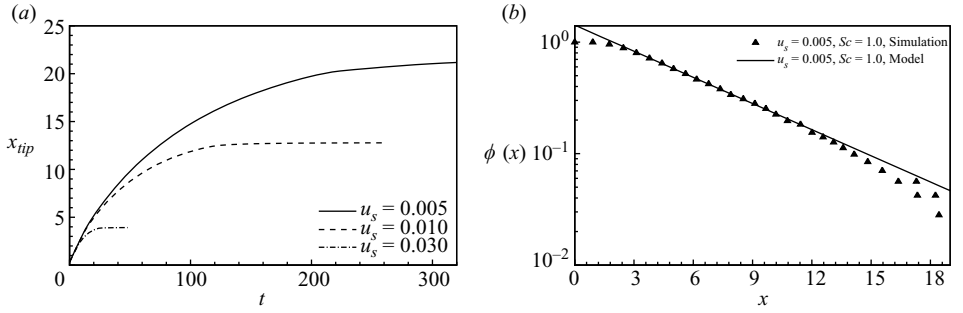

FIGURE 5. (*a*) tip location x_{tip} of the overflow current as function of time for various settling speeds, at $Re = 2000$ and $Sc = 1$. Steady states are reached at $t = 35$, 130 and 240, respectively. (*b*) comparison of model prediction (solid line) and simulation results (triangles) for $u_s = 0.005$ and $Sc = 1$. Good agreement is observed for the interval in which entrainment is negligible.

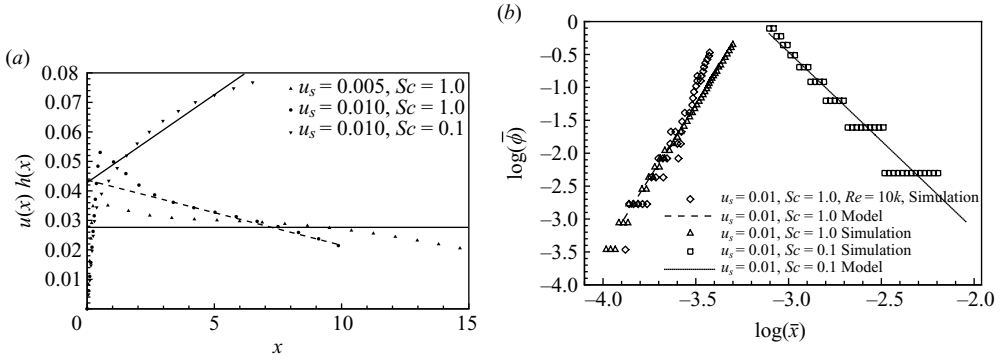

FIGURE 6. (*a*) $u(x)h(x)$ vs x from the numerical simulations. Linear fits of the data give $uh = 0.0278$ for $(u_s, Sc) = (0.005, 1)$, $uh = -0.0022x + 0.0437$ for $(0.01, 1)$ and $uh = 0.0059x + 0.043$ for $(0.01, 0.1)$. (*b*) comparison of model predictions (lines) and simulation results (symbols) for flows with approximately constant entrainment or detrainment. The agreement is satisfactory in those regions where the entrainment rate is approximately constant.

assume the steady state to have been reached when the tip velocity has decreased to 0.01. Accordingly, the steady states are established at times 35, 130 and 240, respectively, for settling velocities of 0.03, 0.01 and 0.005.

5. Comparison of model predictions and simulation results

As a first step, we need to further process the simulation results in order to extract information on $h(x)$, $\phi(x)$ and $u(x)$. These quantities are defined, respectively, as

$$h(x) = \int_0^1 \frac{c(x, y)}{c(x, 0)}\, dy,\ \phi(x) = \frac{1}{h(x)} \int_0^{h(x)} c(x, y)\, dy \text{ and } u(x) = \frac{1}{h(x)} \int_0^{h(x)} u(x, y)\, dy. \tag{5.1}$$

In the case of low entrainment, when uh is approximately constant, the simulation results are to be compared to equation (2.5). For an approximately constant rate of entrainment uh should vary linearly with x, and the results should be compared with equation (2.7).

Figure 6(*a*) shows the variation of $u(x)h(x)$ with x for the simulations with $(u_s, Sc) = (0.005, 1)$, $(0.01, 1)$ and $(0.01, 0.1)$. Symbols indicate the simulation results,

while lines show linear fits. For $(0.005, 1)$, the value of $u(x)h(x)$ is approximately constant in the interval $3 < x < 12$, indicating that very little entrainment takes place. For $(0.01, 1)$, $u(x)h(x)$ exhibits an approximately linear decrease for $3 < x < 10$, as a result of a nearly constant detrainment. In contrast, the case $(0.01, 0.1)$ gives rise to nearly constant entrainment, resulting in an approximately linear increase of $u(x)h(x)$ in the region $2 < x < 5$.

For the case of $(u_s, Sc) = (0.005, 1)$, a linear fit of the data gives $uh = A_0 = 0.0278$, so that equation (2.5) yields $\phi(x) \sim e^{-0.18x}$. This result is shown in figure 5(b) as a solid line, while the triangle symbols represent the corresponding simulation results for $\phi(x)$. Very good agreement is observed over the interval for which figure 6(a) had indicated approximately negligible entrainment. Similarly, we obtain for $(u_s, Sc) = (0.01, 1)$ that $E(x) = -0.0022$ and $uh = -0.0022x + 0.0437$. Equation (2.7) yields $\phi(\overline{x}) \sim \overline{x}^{3.55}$, where $\overline{x} = -0.0022x + 0.0437$. Figure 6($b$) indicates good agreement of simulation data and model predictions for the x-interval in which the model can be expected to apply. Finally, for the positive entrainment case $(u_s, Sc) = (0.01, 0.1)$ we obtain $E(x) = 0.0059$ and $uh = 0.0059x + 0.043$, so that equation (2.7) predicts $\phi(\overline{x}) \sim \overline{x}^{-2.7}$, where $\overline{x} = 0.0059x + 0.043$. Again, figure 6($b$) shows good agreement. Furthermore, note that an increase in Re from 2000 to 10 000 does not change the results significantly. Overall, we observe that in all cases the model provides acceptable predictions for the levee shapes. Deviations are mostly limited to the root and/or the tip of the overflow current, where the vertical velocities cannot be neglected.

In conclusion, the present investigation develops a simple shallow water model for the overflow currents that govern the levee formation, based on a steady state balance of sediment supply by the turbidity current, and sediment deposition onto the levee. The model demonstrates that entrainment is the determining factor for the levee shape, a result that is confirmed by two-dimensional, unsteady Navier–Stokes simulations.

We acknowledge financial support from a consortium of oil companies including BG Group, BP, BHP Billiton Petroleum, Chevron, ConocoPhillips, Hydro, Hess, Maersk Oil, Marathon Oil, Murphy Oil, Petrobras, Statoil and Total, as well as the assistance of Nicolas Guillaume in performing some of the simulations.

REFERENCES

Babonneau, N., Savoye, B., Cremer, M. & Klein, B. 2002 Morphology and architecture of the present canyon and channel system of the Zaire deep-sea fan. *Mar Petrol Geol* **19**, 445–467.

Beghin, P., Hopfinger, E. J. & Britter, R. E. 1981 Gravitational convection from instantaneous sources on inclined boundaries. *J. Fluid Mech.* **107**, 407–422.

Birman, V. K., Battandier, B. A., Meiburg, E. & Linden, P. F. 2007 Lock exchange flows in sloping channels. *J. Fluid Mech.* **577**, 53–77.

Blanchette, F., Strauss, M., Meiburg, E., Kneller, B. & Glinsky, M. E. 2005 High-resolution numerical simulations of resuspending gravity currents: conditions for self-sustainment. *J. Geophys. Res.* **110**, C12022.

Bonnecaze, R., Huppert, H. E. & Lister, J. R. 1993 Particle-driven gravity currents. *J. Fluid Mech.* **250**, 339.

Bonnecaze, R. & Lister, J. 1999 Particle-driven gravity currents down planar slopes. *J. Fluid Mech.* **390**, 75.

Bowen, A. J., Normark, W. R. & Piper, D. J. W. 1984 Modelling of turbidity currents on the navy submarine fan, California continental borderland. *Sedimentology* **31**, 169–185.

Britter, R. & Linden, P. 1980 The motion of the front of a gravity current travelling down an incline. *J. Fluid Mech.* **99**, 531.

Clark, J. D. & Pickering, K. T. 1996 *Submarine Channels, Processes and Architecture*. Vallis Press, London.

Dade, W. B., Lister, J. R. & Huppert, H. E. 1994 Fine-sediment deposition from gravity surges on uniform slopes. *J Sed Res* A **64**, 423–432.

Hallworth, M. A., Phillips, J. C., Huppert, H. E. & Sparks, S. J. 1993 Entrainment in turbulent gravity currents. *Nature* **362**, 829–831.

Härtel, C., Meiburg, E. & Necker, F. 2000 Analysis and direct numerical simulation of the flow at a gravity-current head. part 1. flow topology and front speed for slip and no-slip boundaries. *J. Fluid Mech.* **418**, 189.

Hiscott, R. N., Hall, F. R. & Pirmez, C. 1997 Turbidity-current overspill from the Amazon channel; texture of the silt/sand load, paleoflow from anisotropy of magnetic susceptibility and implications for flow processes. *Proceedings of the Ocean Drilling Program* **155**, 53–78.

Huebscher, C., Spiess, V., Breitzke, M. & Weber, M. E. 1997 The youngest channel–levee system of the Bengal fan; results from digital sediment echosounder data. *Mar. Geol.* **141**, 125–145.

Huppert, H. E. 1998 Quantitative modeling of granular suspension flows. *Phil. Trans. R. Soc. Lond. A.* **356**, 2471.

Kane, I. A., Kneller, B. C., Dykstra, M., Kassem, A. & McCaffrey, W. D. 2007 *Anatomy of a Submarine Channel Levee: an Example from Upper Cretaceous Slope Sediments, Rosario Formation*, Baja California, Mexico. *Mar. Petrol Geol.* **24**, 540–563.

Kolla, V. & Schwab, A. M. 1995 *Atlas of Deep Water Environments; Architectural Style in Turbidite systems (Indus fan: multi-channel seismic reflection images of channel–levee-overbank complexes)*. Chapman & Hall.

Necker, F., Härtel, C., Kleiser, L. & Meiburg, E. 2002 High-resolution simulations of particle-driven gravity currents. *Int. J. Multiphase Flow* **28**, 279–300.

Necker, F., Härtel, C., Kleiser, L. & Meiburg, E. 2005 Mixing and dissipation in particle-driven gravity currents. *J. Fluid Mech.* **545**, 339.

Normark, W. R. & Piper, D. J. W. 1991 Initiation processes and flow evolution of turbidity currents; implications for the depositional record. In *From shoreline to abyss; contributions in marine geology in honor of Francis Parker Shepard* (ed. R. H. Osborne), pp. 207–230. SEPM Spec. Publ. 46.

Normark, W. R., Posamentier, H. & Mutti, E. 1993 Turbidite systems; state of the art and future directions. *Rev Geophys* **31**, 91–116.

Piper, D. J. W. & Savoye, B. 1993 Processes of late quaternary turbidity current flow and deposition on the Var deep-sea fan, north-west Mediterranean sea. *Sedimentology* **40**, 557–582.

Pirmez, C. & Imran, J. 2003 Reconstruction of turbidity currents in Amazon channel. *Mar Petrol Geol* **20**, 823–849.

de Rooij, F. & Dalziel, S. B. 1998 Time-resolved measurements of the deposition under turbidity currents. In *Proceedings of the Conference on Sediment Transport and Deposition by Particulate Gravity Currents, Leeds*.

Skene, K. I., Piper, D. J. W. & Hill, P. S. 2002 Quantitative analysis of variations in depositional sequence thickness from submarine channel levees. *Sedimentology* **49**, 1411–1430.

Srivatsan, L., Lake, L. W. & Bonnecaze, R. T. 2004 Scaling analysis of deposition from turbidity currents. *Geo-Mar. Lett.* **24**, 63.

Turner, J. S. 1968 The influence of molecular diffusivity on turbulent entrainment across a density interface. *J. Fluid Mech.* **33**, 639–656.

Turner, J. S. 1986 Turbulent entrainment: the development of the entrainment assumption, and its application to geophysical flows. *J. Fluid Mech.* **173**, 431.